



# Short carbon fiber-reinforced PLA composites: influence of 3D-printing parameters on the mechanical and structural properties

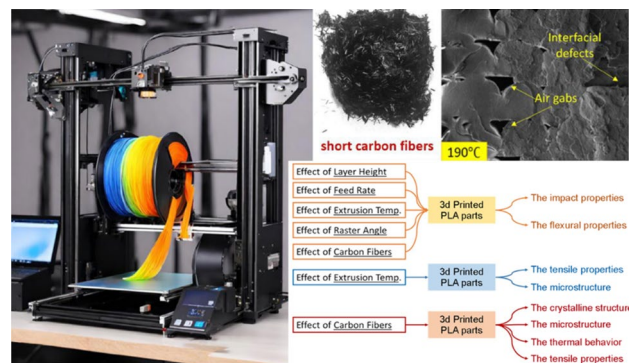
Rasha Alkabbanie<sup>1</sup> · Bulent Aktas<sup>1</sup> · Gokhan Demircan<sup>1</sup> · Serife Yalcin<sup>2</sup>

Received: 3 October 2023 / Accepted: 20 January 2024 / Published online: 15 April 2024  
© The Author(s) 2024

## Abstract

3D printing, particularly “fused filament fabrication” (FFF), plays a crucial role in Industry 4. FFF is widely used for creating complex structures and multi-material parts across various industries such as food industry, fashion industry, and manufacturing sectors. The properties of FFF-produced objects are remarkably affected by printing parameters. This study explores the impact of printing parameters and the addition of short carbon fibers on the strength of polylactic acid (PLA) printed samples. The lowering layer height, increasing feed rate and extrusion temperature boost impact strength, while a smaller raster angle enhances it. Meanwhile, an improved flexural strength is achieved by adjusting layer height, extrusion temperature, and raster angle. Higher extrusion temperatures enhance tensile strength, microstructure, and reduce porosity. Lower layer height improves flexural and impact strength (28.05% increase in 0.1 mm layer height), higher feed rate boosts strengths (12.56% improvement in 7 mm<sup>3</sup>/s feed rate), and elevated extrusion temperatures enhance impact strength (14.49% increase in 230 °C extrusion temperature) but reduce flexural strength (14.44% decrease). Incorporating carbon fibers in PLA negatively affects the microstructure but increases crystallinity, raising the melting temperature and lowering cold-crystallization temperature. The introduction of carbon fibers into PLA results in a complex interplay of mechanical and thermal properties.

## Graphical abstract



**Keywords** Carbon fiber · PLA composite · Printing parameters · Mechanical properties · Thermal properties

✉ Gokhan Demircan  
gdemircan@harran.edu.tr

<sup>1</sup> Department of Mechanical Engineering, Engineering Faculty, Harran University, Sanliurfa, Turkey

<sup>2</sup> Department of Physics, Arts and Science Faculty, Harran University, Sanliurfa, Turkey

## Introduction

Polymer materials play a pivotal role in modern industries [1, 2]. They are recognized for their versatile properties, including durability, lightweight nature, and customizable

functionalities [3–5]. Polymers have a significant application in biocomposites, where natural additives combine with synthetic polymers [6, 7]. This combination creates materials with enhanced mechanical properties with lower environmental impact [8, 9]. Biocomposites find applications in various sectors, such as automotive, construction, and packaging, contributing to sustainable practices in material utilization [10–12]. The production methods of polymer materials have evolved significantly, incorporating advanced techniques like extrusion, injection molding, and compression molding. Notably, the emergence of 3D printing technology has revolutionized polymer manufacturing, allowing for precise and intricate designs.

It is undeniable that 3D printing technology has undergone remarkable advancements in the past decade, revolutionizing the production of objects, including the production of polymer materials across various applications. This cutting-edge technology has played a pivotal role in what is commonly referred to as the recent industrial revolution, where manufacturers leverage information, digitization, and connectivity to optimize their production processes. The 3D printing technologies have many advantages such as mass customization, unlimited designs, waste reduction, and capability to produce complex structures [13, 14]. The technologies have become increasingly accessible to both designers in the market and industry professionals, as well as the general public [15]. Nowadays, thermoplastics, graffiti materials, ceramics, composite materials, and metals can be used for producing parts by 3D printing technologies. The wide variety of materials involved in 3D printing has led to a wider spread of this technology in industry and market [16].

3D printing comprises a broad array of additive manufacturing technologies. Basically, there are four major categories of 3D printing technologies. They are liquid-based technologies, powder-based technologies, solid-based technologies, and paper-based technologies [17]. A diverse array of 3D printing technologies exists, including but not confined to “laminated object manufacturing”, “direct laser sintering” and “fused filament fabrication” (FFF) [18]. One that is more accessible to public is FFF. This technology has provoked industrial innovations by enabling users to have feasible and efficient solutions for producing high-performance functional objects with complex geometries [19]. The materials that are mostly used with FFF include acrylonitrile–butadiene–styrene (ABS) and polylactic acid (PLA) [20–22].

In 3D printing of an item using FFF technology, it is crucial to specify the appropriate parameters for optimal results. The quality of the printed objects varies by changing the 3D-printing parameters such as extrusion temperature, nozzle radius, layer height, printing velocity, infill density, feed rate, and raster angle [23]. Recently, many studies have been conducted to investigate the effect of

printing parameters on the properties of fabricated parts. Liu and Ciftci [24] investigated the effects of 3D-printing parameters on the tensile properties of the carbon fiber and glass fiber-reinforced PEEK objects. It was found that the tensile strength and the flexural strength were improved by raising the values of nozzle and platform temperature. Whereas, using a higher layer thickness and printing speed did result in deteriorating the mechanical properties. The mechanical properties of a PET-G material were tested [25]. The samples were fabricated using variant filling structures (rectilinear, honeycomb, and triangular). The results revealed that the values of tensile strength and elongation of the rectilinear-filling parameters were higher than the full honeycomb and the triangular ones. Furthermore, samples were produced by 3D printing using different printing infill ratios (80%, 50%, and 20%) in the study [26]. It was found that when the infill ratio increases, the elongation averages decline whereas the tensile strengths become greater.

The influence of the layer height and the binder saturation on test samples, produced by 3D printing technology on ZCorp’s Z510/cx, was investigated [27]. The results showed that using lower binder saturation resulted in less tensile strength and integrity, while using lower values of the layer thickness for printing led to higher tensile strengths and less flexural strengths. Using fused-deposition technology, the PLA specimens were printed and tested to determine the flexural properties [28]. Test results revealed that the maximum flexural strength considerably have risen when adding more thickness to the layer and the tensile strength declined and then increased when using larger values of the layer height. Also, the study showed that the 90-degree delamination fracture while in the case of using thinner layers, the specimens showed 45-degree delamination fracture to the printing path.

Numerous studies have also investigated the effects of incorporating carbon fibers into PLA filaments. PLA materials were produced using carbon fiber with higher tensile characteristics [29]. However, according to a different study [30], carbon fibers reduced PLA sample hardness by 68% and strain by 65%. The carbon fibers significantly (approximately 2.2 times) increased the tensile modulus and made the material more brittle [31].

In the existing literature, a noticeable gap is apparent as there are no studies exploring the influence of 3D-printing parameters on the impact properties of carbon fiber-reinforced PLA printed parts. In addition, a lack of research is evident in simultaneously examining the effects of layer height, feed rate, extrusion temperature, and raster angle parameters. To address this gap, our research conducts mechanical and structural tests on samples printed with varying layer thicknesses, extrusion temperatures, feed rates and raster angles.

## Experimental

### Materials

The FFF filament material, for production of test samples as biodegradable thermoplastics was PLA. The material has good mechanical strength, minimal toxicity, and it is biocompatible [32]. PLA is widely used in medical applications such as wounding management, drug delivery, orthopedic and fixation devices, tissue engineering, and re-engineering medicine [33]. The commercial name of the filament material is Tier time PLA (1.75 mm, 500 g) and the manufacturer is Up Fila (China). The mechanical specifications of this material are listed in Table 1.

The PLA + CF composite filament is purchased from the same company and produced using the same PLA matrix adding 15% (by wt) of the carbon fibers (short, 12 μm diameter).

### Samples preparation

In this study, the samples were 3D printed using FFF technology in which the material is dragged through a nozzle where it is heated till it melts and extruded onto the work piece. The nozzle tracks a path defined by CAD/CAM file under the computer control. The material is deposited successively until the part is completed. The printer used in producing the samples is “Up Box” 3D printer.

Test samples were designed as 3D models using Solid Works software, and the model data were given into the slicing software. Some printing parameters were fixed for all the samples such as filament diameter (1.75 mm), nozzle diameter (0.5 mm), printing speed (50 mm/s) and filling structure (rectilinear) while others varied to show the effect of these parameters on the mechanical strengths [34]. Table 2 gives 3D-printing parameters. In addition, to better understand the structure of this study, schematic representation of the variable parameters and the tests are shown in Fig. 1.

### Tests

The aim of impact test is to define the material impact strength when subjected to impact force. This dynamic test was performed as per the standard ASTM D6110-18 using

**Table 1** Mechanical properties of PLA

Property	Metric
Tensile strength	> = 60 MPa
Flexural strength	31.5 MPa
Elongation-at-break	4.4–6%

**Table 2** Printing parameters

Notations	Layer height (mm)	Feed rate (mm <sup>3</sup> /s)	Extrusion temperature (°C)	Raster angle (degree)
PLA-L0.1	0.1	7	190	30
PLA-L0.2	0.2	7	190	30
PLA-L0.3	0.3	7	190	30
PLA-F7	0.1	7	190	30
PLA-F8	0.1	8	190	30
PLA-F9	0.1	9	190	30
PLA-E190	0.1	7	190	30
PLA-E210	0.1	7	210	30
PLA-E230	0.1	7	230	30
PLA-R30	0.1	7	190	30
PLA-R60	0.1	7	190	60
PLA-Pure	0.1	7	230	30
PLA + CF	0.1	7	230	30

Avery Dennison (USA) impact-testing device. In this test, the pendulum is released from the upper position to give a striking energy. The scale carries a set of gradations. The sample is clamped horizontally. Equation 1 is applied to calculate the impact strength.

$$R = \frac{W.L.(\cos \alpha - \cos \beta)}{A}, \tag{1}$$

where  $R$  is impact strength (kJ/m<sup>2</sup>);  $W$  is pendulum weight (kg);  $L$  is pendulum length (m);  $\alpha$  is angle of fall (before impact);  $\beta$  is angle at the end of the swing (after impact);  $A$  is area of cross-section of the sample where the break appears.

The samples were subjected to the flexural test according to the ASTM D790 Standard. All the samples were tested using the same loading rate. The test is stopped when the sample is broken.

Flexural strength is found using Eq. 2.

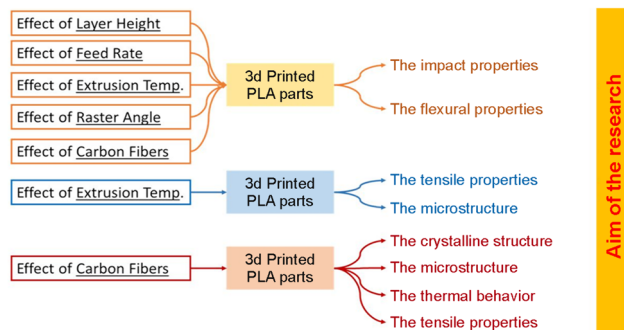


**Fig. 1** Schematic representation of variable parameters and of the tests

$$\sigma_f = \frac{3FL}{2bd^2}, \quad (2)$$

where  $\sigma_f$  is flexural strength (Pa);  $F$  is applied force (N);  $L$  is support span length (m);  $b$  is width of the object (m);  $d$  is height of the object (m).

A Shimadzu AGS-X Plus Universal Tensile machine (Japan) was used to conduct the tensile test (ASTM D638). A highly accurate non-contact digital video extensometer was used to measure the stress values. According to ISO 9513 Class 0.5 and JIS B 7741 Class 0.5, it offered measurements for elongation with high precision.

The Perkin & Elmer DSC 8000 (USA) equipment was used to analyze data using differential scanning calorimetry (DSC). For analysis, the samples weighing 5 mg were put in the aluminum pan and sealed. Using the empty pan, the enthalpy change, and melting point were monitored. A nitrogen environment with a flow rate of 50 mL/min was used for the test. The measurements were performed with heating rates of 10 °C/min from 30 to 200 °C and cooling rates of -10 °C/min from 200 to 30 °C. Using 40 kV and 30 mA with CuK $\alpha$  radiation at 0.02 scanning speed, the XRD spectra of the PLA and PLA + CF samples were obtained (Rigaku-Dmax 2000 X-Ray diffractometer, Japan). The fracture surface of the tensile samples was examined using a Zeiss Evo 50 device scanning electron microscope operating at 20 kV.

## Results and discussion

### Impact test results

The impact of the printing parameters is illustrated in Fig. 2. As it can be realized, increasing the layer height resulted in a decline in the impact strength, while, increasing the feed rate and the extrusion temperature raised the value of the impact strength. This can be explained by the knowledge that using lower layer heights results in a larger crystal content and smaller crystals [35]. Lower layer heights can contribute to smaller crystal content. When layers are deposited with smaller thicknesses, the cooling rate becomes higher, promoting faster crystallization. Smaller crystal content can affect the material's mechanical properties, as the arrangement and size of crystals play a role in determining strength and toughness [35]. Also, the decline in the impact strength when using a larger raster angle can be interpreted by the higher air gap among the layers for the samples printed with higher raster angle [36] and also the smaller raster angles exhibit strong interlayer bonding [37]. Higher amount of heat applied when utilizing a higher extrusion temperature improves the diffusion that takes place at the joining interface between the rasters. The stronger bonding between the adjacent raster results in higher impact strength [37]. Also,

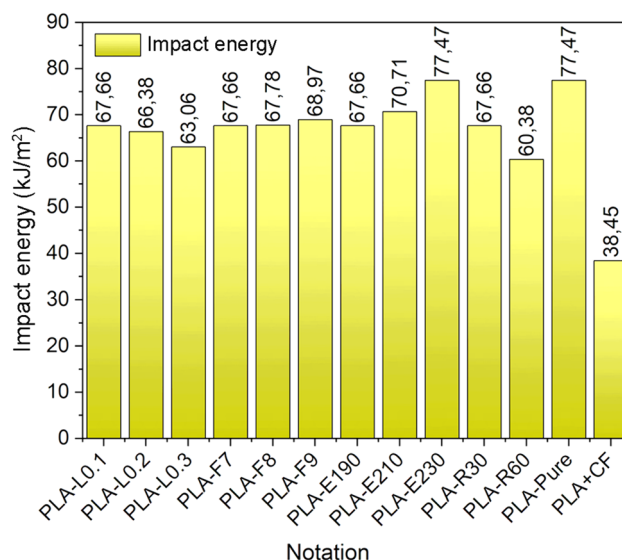


Fig. 2 Impact test results

a thinner layer leads to tightly coalesced interlamination which is caused by a squeeze of nozzle, and this causes the rise in the impact strength [38]. In conclusion, a higher feed rate increases infill density, enhancing energy absorption. Objects with thinner layer heights take more time to construct, allowing prolonged exposure above  $T_m$  for improved interfacial diffusion. A lower crystal size has the potential to decrease both strained amorphous fraction and internal flaws in spherulites. These findings highlight the intricate relationship between feed rate, layer height, and crystal size in additive manufacturing processes [35].

### Flexural test results

The results of the flexural tests are illustrated in Fig. 3. Experimental results displayed in the charts clearly demonstrated a relationship between the parameter being changed and the sample's flexural strength. The flexural strength increases using smaller layer heights, lower extrusion temperatures, and larger raster angles. As the temperature is increased from 190 to 230 °C, flexural strength is dropped from 59.06 to 50.53 MPa. Increased-extrusion temperature allows polymer chains to have greater kinetic energy, promoting better molecular alignment and crystallinity. Improved-molecular alignment contributes to a more ordered and structurally sound material, resulting in increased flexural strength.

Whereas the flexural strength is increased from 59.06 to 66.48 MPa when escalating the feed rate from 7 to 8 mm<sup>3</sup>/s but it is declined to 55.65 MPa when using a feed rate of 9 mm<sup>3</sup>/s. The reason for this decrease may be higher and the feed rates might result in rougher surfaces. Surface roughness can act as a stress concentrator, promoting

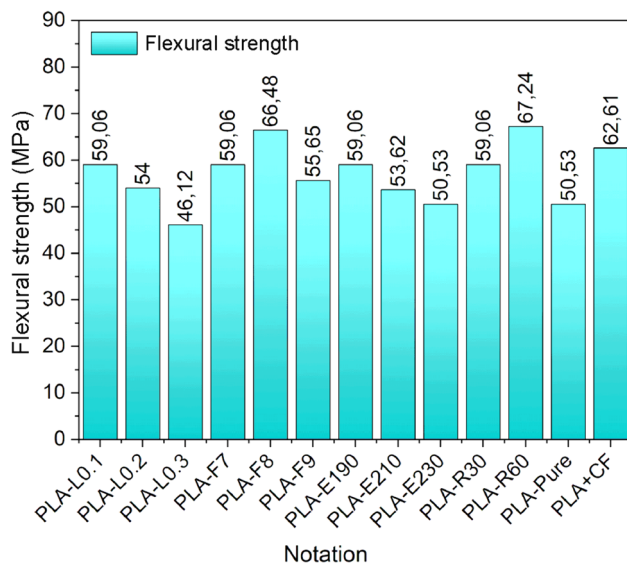


Fig. 3 Flexural test results

the initiation and propagation of cracks, which ultimately leads to a reduction of flexural strength directly related to the surface [39]. High feed rates may lead to increased surface roughness. The presence of rough surfaces can act as stress concentrators. Stress concentrations arise at points of geometric irregularities, and these concentrated stresses can initiate and propagate cracks, ultimately reducing the material's flexural strength.

Lower values of the layer height produce higher integrity, which in turn boosts the specimens' strength. In addition, utilizing thinner layers results in a smaller air gap to material ratio, where the breaking point is reached at greater loads [40]. Delamination is also frequently seen in parts printed at lower raster angles, and this causes stress fluctuation [41].

### Tensile test results

As can be seen in Fig. 4, the maximum tensile strength showed an obvious dependence on the extrusion temperature. Temperature plays a critical role in the quality of bonding between layers. Higher temperatures generally enhance interlayer adhesion, reducing porosity and improving the overall mechanical properties of the printed composite [42]. Conversely, lower temperatures can lead to inadequate bonding, increasing the likelihood of porosity and reducing the tensile strength of the material [43]. The relationship between temperature, bonding, and porosity is a key consideration in optimizing 3D-printing parameters for short carbon fiber-reinforced PLA composites to achieve desired mechanical and structural properties.

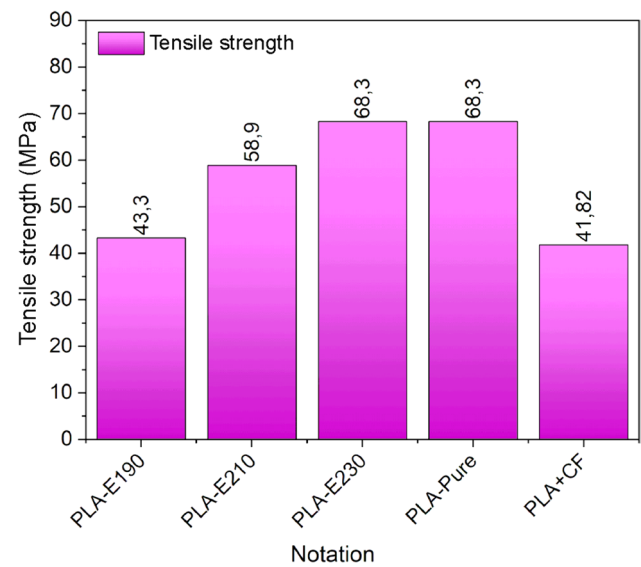


Fig. 4 Tensile test results

### Microstructure analysis

The effect of extrusion temperature on interfacial bonding is detected and confirmed by SEM images of the tensile fracture surface (Fig. 5). Specimens with various extrusion temperatures have various microstructures at their fractured surfaces. When printed with lower extrusion temperatures of 190 °C, as demonstrated in Fig. 5, noticeable interfacial flaws, and voids (porosity) are seen in the internal specimens. The decrease in the maximum tensile strength shown in the previous section can be attributed to these faults because they are detrimental to stress transmission. Low-void fraction is attained at higher extrusion temperatures (210 °C and 230 °C), indicating improved interfacial adhesion between printing interlayers. It is clear from this that the extra porosity and interfacial bonding of PLA printed objects are discovered to be temperature dependent. The findings are well in line with the research [38, 44]. At lower temperatures, there could be a lack of deposition leading to larger air gap, which results in a reduced load-bearing cross-sectional area under a uniaxial tensile load, while reducing the strength of the parts.

### The effect of short carbon fibers on mechanical properties

A comparison between the PLA specimen and the PLA + CF specimen printed using the same printing parameters was conducted. The impact, flexural and tensile test results are shown in Figs. 2, 3, and 4, respectively. The microstructure analysis is illustrated in Fig. 5. While the maximum strength is decreased in the impact and tensile test, but it is increased



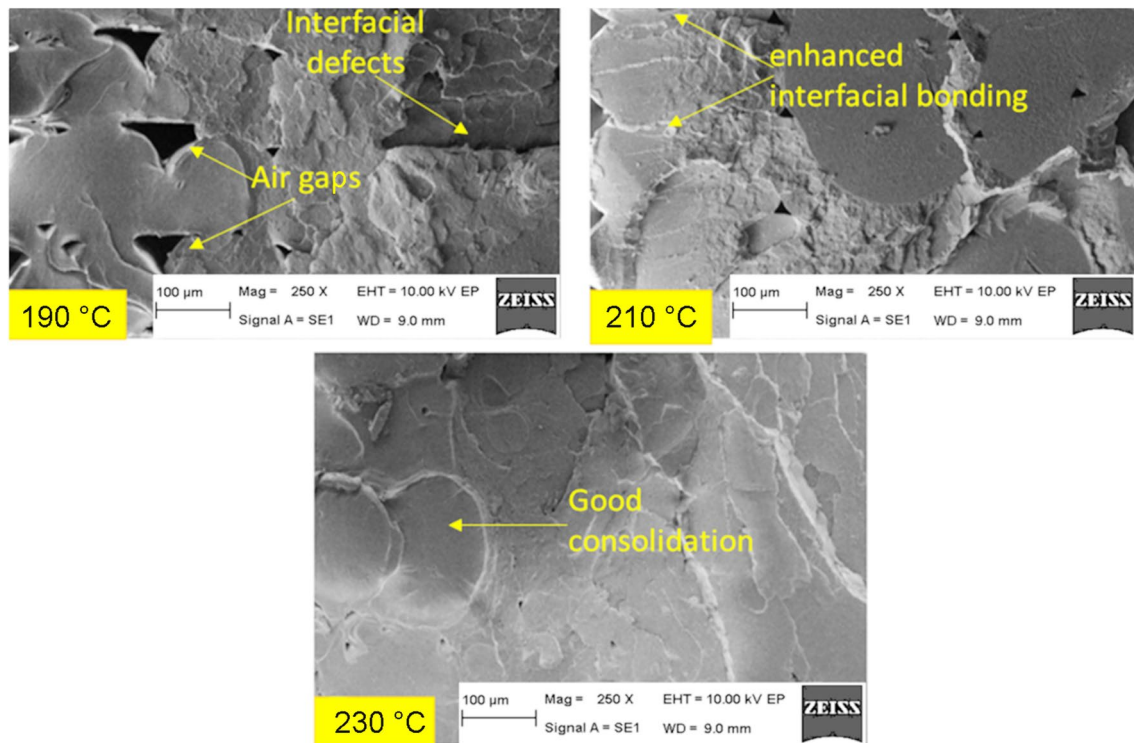


**Fig. 5** SEM images of tensile test fracture surface

in the flexural test. Short carbon fibers, as opposed to longer ones, may not provide as effective energy-dissipation mechanisms during impact events. The limited length of the fibers may result in less bridging between crack surfaces, reducing the material's ability to absorb impact energy. The introduction of short carbon fibers can create stress concentrations within the composite material. Irregularities at the fiber ends or interfaces can act as points of stress concentration, contributing to the initiation and propagation of cracks, which in turn reduces the overall tensile strength of the material [38]. Another reason for the decrease might be that the carbon fibers have a high-thermal conductivity that changes the thermal gradient, resulting in a change in the viscosity and cooling rate of the molten filament that inhibits PLA flow and causes air gaps between the rasters. In addition, shrinkage in fiber-reinforced materials is higher than in unfilled materials. In bending, the short carbon fibers may act as reinforcing elements that support the matrix material. This reinforcement can counteract the tensile stresses generated on the convex side of the bend, contributing to improved bending strength [45].

CF has increased strength in flexural test. This is because of crack bridging. When the PLA composite is subjected to flexural stress, microcracks develop in the matrix. The carbon fibers have the ability to bridge these cracks, preventing them from propagating further. This crack-bridging mechanism effectively increases the toughness and resistance to

flexural failure, contributing to the overall flexural strength improvement.

The SEM images shown in Fig. 6 support the mechanical test results. The size of the gaps of PLA + CF samples is much larger than the PLA samples which possess more bonding. The FFF process involves the layer-by-layer deposition of material. During this process, the molten-PLA material partially penetrates the surface irregularities of the carbon fibers, creating a form of mechanical interlocking. This interlocking contributes to the overall adhesion between the fibers and the matrix [46]. In addition, during the FFF process, the PLA material may partially wrap around the untreated carbon fibers, leading to physical entanglement. This entanglement enhances the mechanical interlocking effect and contributes to the overall stability of the fiber–matrix interface. The SEM images explain well the results of the tensile test and the impact test which indicate that the PLA-CF samples, fractured under a tensile stress and impact shock, are much less than the PLA samples. The enhanced bonding of printing interlayers in the PLA sample contributes to an effective stress transfer, which explains the enhanced tensile properties.

### The effect of short carbon fibers on XRD

Figure 7 shows the X-ray diffraction (XRD) patterns of PLA and PLA + CF composite. PLA polymers exhibit a diverse

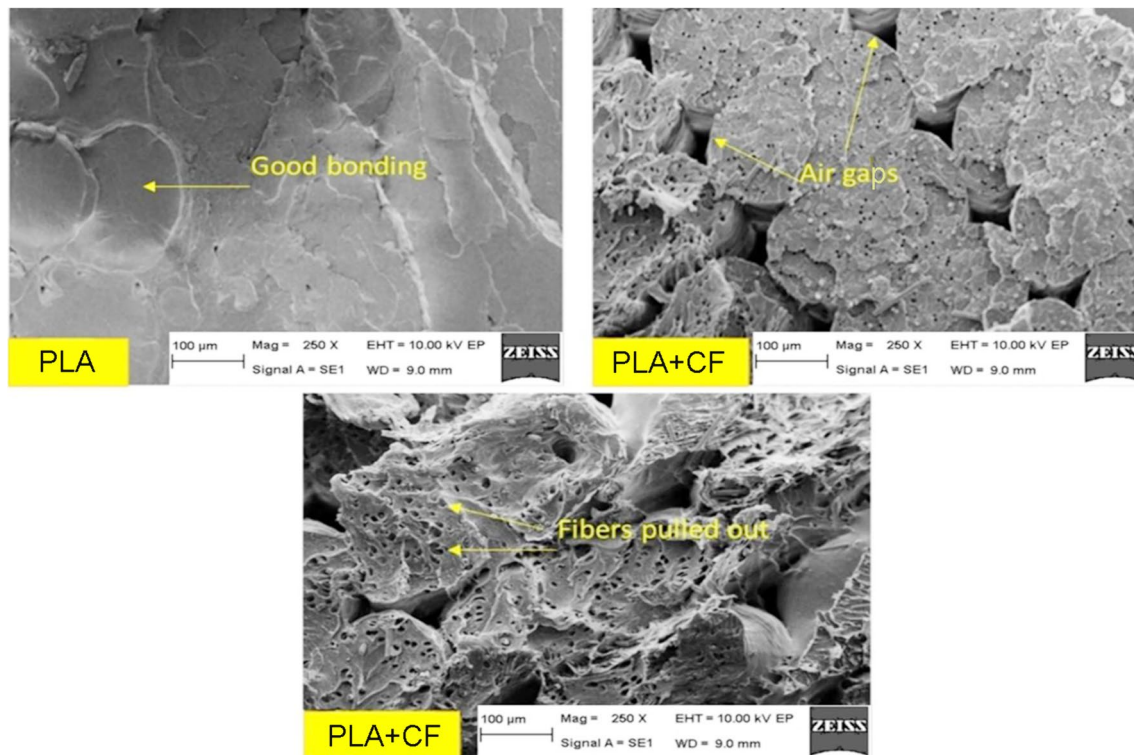


**Fig. 6** The microstructure comparison between PLA and PLA + CF

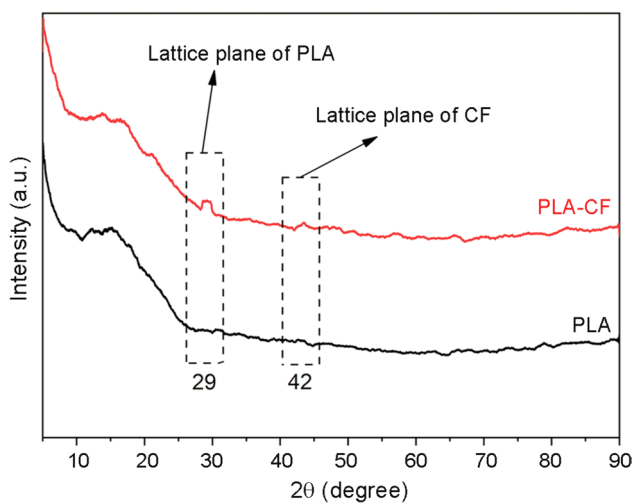


**Fig. 7** XRD-test results of PLA and PLA + CF samples

range of properties, spanning from amorphous and glassy characteristics to semi-crystalline structures, and even highly crystalline formation [47, 48]. The neat PLA has exhibited no peaks, showing its amorphous nature [49–51]. However, the composite shows peaks at around  $2\theta$  equals to 29 and 42, which correspond to the (216) lattice plane of PLA (PDF (00–054–1917)  $(C_3H_5O_3)_n$ - $\alpha$ -poly(D-lactide) and (020) of

carbon (PDF (00–054–0501)  $C$  – carbon)). This indicates that the composite has more crystalline structure. From the X-ray patterns, it could be confirmed that the addition of CF has advanced the crystallization of PLA. In addition, the reason for the background noise is that the carbon fiber is not distributed completely homogeneously within the PLA.

Three basic crystal phases of  $\alpha$ ,  $\beta$ , and  $\gamma$  and as well as a secondary, less stable, disordered  $\alpha'$  phase are present in PLA [52]. A slow cooling process used to create the common crystallite form from the melt enables the PLA chain to rotate into the confirmation with less potential energy [53]. The  $10^3$  helicoidal conformation (containing 10 helix repeat structures in three chain twists) packed in an orthorhombic unit cell is what distinguishes the polymorphicity [54].

### The effect of short carbon fibers on thermal behavior

Figure 8 displays the DSC heat flow–temperature graphs for PLA and the PLA + CF samples. A melting peak was seen in the PLA sample at 167 °C, which was followed by cold crystallization at roughly 75 °C. A melting peak was observed in the PLA + CF sample at 172 °C, while the PLA sample displayed cold crystallization at roughly 70 °C. The glass-transition temperature was measured as 58 °C for PLA and 56 °C for PLA + CF. Due to the enhanced mobility during

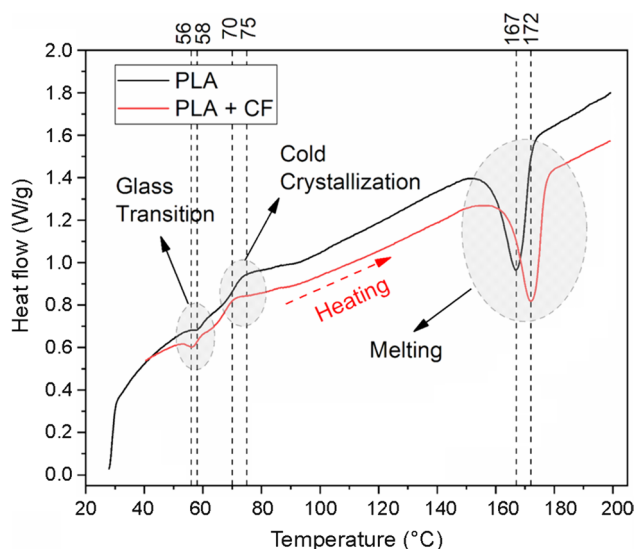


**Fig. 8** DSC-test results of PLA and PLA + CF samples

heating, there is a rearrangement of molecular chains in the crystalline PLA lamellae at the cold transition peaks [29]. The introduction of carbon fiber in the composite has led to an elevation in amorphousness, consequently resulting in a higher melting temperature compared to PLA samples [55]. The homopolymer is difficult to crystallize from a glassy state, as evidenced by low intensity of the cold-crystallization peaks. The cooling curves are nearly identical, in contrast to the heating curve, which appears to be unaffected by the introduction of carbon fiber.

With the addition of carbon fibers, the cold-crystallization temperature of PLA + CF samples is dropped, and this may be explained by the fact that the carbon fiber has acted as a nucleating agent, which encourages crystallinity. It is important to note that the samples with carbon fiber inclusion have a marginally lower glass transition [55].

## Conclusion

This research addresses a notable gap in existing literature by investigating the impact of 3D-printing parameters on the impact properties of carbon fiber-reinforced PLA printed parts. The study uniquely explored the simultaneous effects of layer height, feed rate, extrusion temperature, and raster angle parameters, shedding light on their influence on impact strength, flexural strength, and tensile strength. The research involved mechanical and structural tests on PLA samples printed with varying parameters and incorporates the addition of short carbon fibers.

The findings revealed that decreasing the layer height enhances flexural and impact strength, with the PLA-L0.1 sample exhibiting a remarkable 28.05% improvement in

flexural strength. Increasing feed rate generally boosts flexural and impact strength, with the PLA-F7 sample showing a peak improvement of 12.56% in flexural strength. The evaluation of extrusion temperature indicated that higher values increase impact strength but decrease flexural strength, exemplified by the PLA-E230 sample with a 14.49% increase in impact energy and a 14.44% decrease in flexural strength.

The introduction of carbon fibers to PLA resulted in a complex interplay of mechanical and thermal properties. While carbon fiber reinforcement decreased impact and tensile strength, it has significantly improved flexural strength by 23.9%. The microstructural analysis indicated that carbon fibers acted as nucleating agents, enhancing PLA crystallization and elevating the composite's thermal stability. The composite exhibited a higher melting peak and lower glass-transition temperature, suggesting improvements in thermal properties without a specific emphasis on increasing the glass transition temperature.

In terms of practical applications, the PLA + CF composite is recommended for scenarios where enhanced flexural strength and thermal stability are crucial. Recommendations for further improvement included printing with higher extrusion temperatures, increasing the extrusion rate with encoder feedback for better control, and using a hardened nozzle conducive to efficient heat conduction. Overall, this research contributes valuable insights into optimizing 3D-printing parameters for PLA + CF composites, offering a nuanced understanding of their mechanical and thermal characteristics for potential applications in diverse industries such as aerospace, automotive, and manufacturing, which demand high-performance materials for intricate components.

**Funding** Open access funding provided by the Scientific and Technological Research Council of Türkiye (TÜBİTAK).

**Open Access** This article is licensed under a Creative Commons Attribution 4.0 International License, which permits use, sharing, adaptation, distribution and reproduction in any medium or format, as long as you give appropriate credit to the original author(s) and the source, provide a link to the Creative Commons licence, and indicate if changes were made. The images or other third party material in this article are included in the article's Creative Commons licence, unless indicated otherwise in a credit line to the material. If material is not included in the article's Creative Commons licence and your intended use is not permitted by statutory regulation or exceeds the permitted use, you will need to obtain permission directly from the copyright holder. To view a copy of this licence, visit <http://creativecommons.org/licenses/by/4.0/>.

## References

- Demircan G, Kisa M, Ozen M, Acikgoz A, İşiker Y, Aytaç E (2023) Nano-gelcoat application of glass fiber reinforced polymer composites for marine application: Structural, mechanical, and thermal analysis. *Mar Pollut Bull* 194:115412



2. Demircan G, Ozen M, Kisa M, Acikgoz A, İşker Y (2023) The effect of nano-gelcoat on freeze-thaw resistance of glass fiber-reinforced polymer composite for marine applications. *Ocean Eng* 269:113589
3. Ozen M, Demircan G, Kisa M, Acikgoz A, Ceyhan G, İşker Y (2022) Thermal properties of surface-modified nano- $\text{Al}_2\text{O}_3$ /Kevlar fiber/epoxy composites. *Mater Chem Phys* 278:125689
4. Demircan G, Kisa M, Ozen M, Aktas B (2020) Surface-modified alumina nanoparticles-filled aramid fiber-reinforced epoxy nanocomposites: preparation and mechanical properties. *Iran Polym J* 29:253–264
5. Demircan G (2024) Structural integrity of glass fiber reinforced nanocomposites under hydrothermal aging for offshore structure applications. *Appl Ocean Res* 146:103959
6. Kulkarni ND, Saha A, Kumari P (2023) The development of a low-cost, sustainable bamboo-based flexible bio composite for impact sensing and mechanical energy harvesting applications. *J Appl Polym Sci* 140:e54040
7. Saha A, Kumari P (2022) Functional fibers from *Bambusa tulda* (Northeast Indian species) and their potential for reinforcing biocomposites. *Mater Today Commun* 31:103800
8. Kumar S, Saha A (2022) Utilization of coconut shell biomass residue to develop sustainable biocomposites and characterize the physical, mechanical, thermal, and water absorption properties. *Biomass Convers Biorefinery*, pp 1–17
9. Saha A, Kumari P (2023) Effect of alkaline treatment on physical, structural, mechanical and thermal properties of *Bambusa tulda* (Northeast Indian species) based sustainable green composites. *Polym Compos* 44:2449–2473
10. Kumar S, Saha A, Bhowmik S (2022) Accelerated weathering effects on mechanical, thermal and viscoelastic properties of kenaf/pineapple biocomposite laminates for load bearing structural applications. *J Appl Polym Sci* 139:51465
11. Kumar S, Saha A (2022) Effects of particle size on structural, physical, mechanical and tribology behaviour of agricultural waste (corn cob micro/nano-filler) based epoxy biocomposites. *J Mater Cycle Waste Manag* 24:2527–2544
12. Kumar S, Saha A, Zindani D (2023) Agro-waste-based polymeric composite laminates for aerospace cabin interior and identification of their optimal configuration. *Biomass Convers Biorefinery*, pp 1–17
13. Candi M, Beltagui A (2019) Effective use of 3D printing in the innovation process. *Technovation* 80–81:63–73
14. Praveena BA, Lokesh N, Buradi A, Santhosh N, Praveena BL, Vignesh R (2022) A comprehensive review of emerging additive manufacturing (3D printing technology): methods, materials, applications, challenges, trends and future potential. *Mater Today Proc* 52:1309–1313
15. Chan HK, Griffin J, Lim JJ, Zeng F, Chiu ASF (2018) The impact of 3D printing technology on the supply chain: Manufacturing and legal perspectives. *Int J Prod Econ* 205:156–162
16. Shahrubudin N, Lee TC, Ramlan R (2019) An overview on 3D printing technology: technological, materials, and applications. *Proc Manuf* 35:1286–1296
17. Megdich A, Habibi M, Laperrière L (2023) A review on 3D printed piezoelectric energy harvesters: Materials, 3D printing techniques, and applications. *Mater Today Commun* 35
18. Kang J, Ma Q (2017) The role and impact of 3D printing technologies in casting. *China Found* 14:157–168
19. Singh S, Singh G, Prakash C, Ramakrishna S (2020) Current status and future directions of fused filament fabrication. *J Manuf Proc* 55:288–306
20. Zanjanijam AR, Major I, Lyons JG, Lafont U, Devine DM (2020) Fused filament fabrication of PEEK: a review of process-structure-property relationships. *Polymers (Basel)* 12:1665
21. Sun C, Wei S, Tan H, Huang Y, Zhang Y (2022) Progress in upcycling polylactic acid waste as an alternative carbon source: A review. *Chem Eng J* 446:136881
22. Xu C, Sun C, Wan H, Tan H, Zhao J, Zhang Y (2022) Microstructure and physical properties of poly(lactic acid)/polycaprolactone/rice straw lightweight bio-composite foams for wall insulation. *Constr Build Mater* 354:129216
23. Schirmeister CG, Hees T, Licht EH, Mülhaupt R (2019) 3D printing of high density polyethylene by fused filament fabrication. *Addit Manuf* 28:152–159
24. Liu L, Ciftci ON (2021) Effects of high oil compositions and printing parameters on food paste properties and printability in a 3D printing food processing model. *J Food Eng* 288:110135
25. Zárbybnická L, Machotová J, Pagáč M, Rychlý J, Vykydalová A (2023) The effect of filling density on flammability and mechanical properties of 3D-printed carbon fiber-reinforced nylon. *Polym Test* 120:107944
26. Ambade V, Rajurkar S, Awari G, Yelamsetti B, Shelare S (2023) Influence of FDM process parameters on tensile strength of parts printed by PLA material. *Int J Interact Des Manuf*, pp 1–12
27. Vaezi M, Chua CK (2010) Effects of layer thickness and binder saturation level parameters on 3D printing process. *Int J Adv Manuf Technol* 53:275–284
28. Nugroho A, Ardiansyah R, Rusita L, Larasati IL (2018) Effect of layer thickness on flexural properties of PLA (polylactic acid) by 3D printing. *J Phys Conf Ser* 1130:12017
29. Magri AEI, El Mabrouk K, Vaudreuil S, Touhami ME (2019) Mechanical properties of CF-reinforced PLA parts manufactured by fused deposition modeling. *J Thermoplast Compos Mater* 34:581–595
30. Rajeshirke M, Alkunte S, Huseynov O, Fidan I (2023) Fatigue analysis of additively manufactured short carbon fiber-reinforced PETG components. *Int J Adv Manuf Technol* 128:2377–2394
31. Ferreira RTL, Amatte IC, Dutra TA, Bürger D (2017) Experimental characterization and micrography of 3D printed PLA and PLA reinforced with short carbon fibers. *Compos Part B Eng* 124:88–100
32. Afrose MF, Masood SH, Iovenitti P, Nikzad M, Sbarski I (2016) Effects of part build orientations on fatigue behaviour of FDM-processed PLA material. *Prog Addit Manuf* 1:21–28
33. Farah S, Anderson DG, Langer R (2016) Physical and mechanical properties of PLA, and their functions in widespread applications—a comprehensive review. *Adv Drug Deliv Rev* 107:367–392
34. Alkabbanie R, Awwad Q (2020) Influence of the printing parameters on the properties of PLA parts produced by fused filament fabrication. *Eurasian J Sci Eng* 6:131–140
35. Wang L, Gardner DJ (2017) Effect of fused layer modeling (FLM) processing parameters on impact strength of cellular polypropylene. *Polymer (Guildf)* 113:74–80
36. Akhouni B, Modanloo V (2023) Investigation and feasibility of printing polyoxymethylene semi-crystalline polymer parts with fused filament fabrication 3D printer and evaluation of mechanical properties of the printed samples. *J Mater Eng Perform*, pp 1–10
37. Rajpurohit SR, Dave HK (2020) Impact strength of 3D printed PLA using open source FFF-based 3D printer. *Prog Addit Manuf* 6:119–131
38. Peng X, Zhang M, Guo Z, Sang L, Hou W (2020) Investigation of processing parameters on tensile performance for FDM-printed carbon fiber reinforced polyamide 6 composites. *Compos Commun* 22:100478
39. Suteja TJ, Soesanti A (2020) Mechanical properties of 3D printed polylactic acid product for various infill design parameters: a review. *J Phys Conf Ser* 1569:42010

40. Ayrimis N, Kariz M, Kwon JH, Kitek Kuzman M (2019) Effect of printing layer thickness on water absorption and mechanical properties of 3D-printed wood/PLA composite materials. *Int J Adv Manuf Technol* 102:2195–2200
41. Lee CS, Kim SG, Kim HJ, Ahn SH (2007) Measurement of anisotropic compressive strength of rapid prototyping parts. *J Mater Proc Technol* 187–188:627–630
42. Mofokeng JP, Luyt AS, Tábi T, Kovács J (2011) Comparison of injection moulded, natural fibre-reinforced composites with PP and PLA as matrices. *J Thermoplast Compos Mater* 25:927–948
43. Auras R, Harte B, Selke S (2004) An overview of polylactides as packaging materials. *Macromol Biosci* 4:835–864
44. Lokesh N, Praveena BA, Reddy JS, Vasu VK, Vijaykumar S (2022) Evaluation on effect of printing process parameter through Taguchi approach on mechanical properties of 3D printed PLA specimens using FDM at constant printing temperature. *Mater Today Proc* 52:1288–1293
45. Maqsood N, Rimašauskas M (2021) Characterization of carbon fiber reinforced PLA composites manufactured by fused deposition modeling. *Compos Part C Open Access* 4:100112
46. Jain A, Kant K, Singh SK, Sahai A, Sharma RS (2023) Process parameter tailored evaluation of FFF-fabricated carbon fibre based poly-lactic-acid composites. *J Thermoplast Compos Mater* 36:4365–4387
47. Lunt J (1998) Large-scale production, properties and commercial applications of polylactic acid polymers. *Polym Degrad Stab* 59:145–152
48. Södergård A, Stolt M (2002) Properties of lactic acid based polymers and their correlation with composition. *Prog Polym Sci* 27:1123–1163
49. Shuhua W, Qiaoli X, Fen L, Jinming D, Husheng J, Bingshe X (2013) Preparation and properties of cellulose-based carbon microsphere/poly(lactic acid) composites. *J Compos Mater* 48:1297–1302
50. Wu D, Samanta A, Srivastava RK, Hakkarainen M (2018) Nanographene oxide functionalized bioactive poly(lactic acid) and poly( $\epsilon$ -caprolactone) nanofibrous scaffolds. *Mater (Basel, Switzerland)* 11:566
51. Silverajah VSG, Ibrahim NA, Yunus WMZW, Hassan HA, Woei CB (2012) A comparative study on the mechanical, thermal and morphological characterization of poly(lactic acid)/epoxidized palm oil blend. *Int J Mol Sci* 13:5878–5898
52. Kuang T, Zhang M, Chen F, Fei Y, Yang J, Zhong M, Wu B, Liu T (2023) Creating poly(lactic acid)/carbon nanotubes/carbon black nanocomposites with high electrical conductivity and good mechanical properties by constructing a segregated double network with a low content of hybrid nanofiller. *Adv Compos Hybrid Mater* 6:1–12
53. Liao Y, Liu C, Coppola B, Barra G, Di Maio L, Incarnato L, Lafdi K (2019) Effect of porosity and crystallinity on 3D printed PLA properties. *Polymers* 11:1487
54. Echeverría C, Limón I, Muñoz-Bonilla A, Fernández-García M, López D (2021) Development of highly crystalline polylactic acid with  $\beta$ -crystalline phase from the induced alignment of electrospun fibers. *Polymers* 13:2860
55. Vinyas M, Athul SJ, Harursampath D, Nguyen Thoi T (2019) Experimental evaluation of the mechanical and thermal properties of 3D printed PLA and its composites. *Mater Res Express* 6:115301